

# Nanostructured LiTaO<sub>3</sub> and KNbO<sub>3</sub> Ferroelectric Transparent Glass-Ceramics for Applications in Optoelectronics

Anal Tarafder and Basudeb Karmakar  
*Glass Science and Technology Section, Glass Division,  
Central Glass and Ceramic Research Institute,  
Council of Scientific and Industrial Research (CSIR, India),  
India*

## 1. Introduction

Ferroelectric bulk crystals are widely used in optoelectronic devices because of their well combination of extraordinary optical and electronic properties. Their crystal structure is non-centrosymmetric and due to this structural anisotropy they exhibit many nonlinear optical properties, for example, the electro-optic effect (change in optical index with electric field), harmonic generation (changing frequency of light), and photorefractive (index change in response to light), to name a few. However, preparation of their defect-free optical quality transparent single crystal is very difficult, lengthy process, and requires sophisticated costly equipment. In recent past, to triumph over these difficulties, much attention has been paid for development of transparent ferroelectric glass-ceramics by the high speed glass technology route because of its low cost of fabrication, tailoring of properties and flexibility to give desired shapes. Lithium tantalate (LiTaO<sub>3</sub>, LT) and potassium niobate (KNbO<sub>3</sub>, KN) single crystals are the most important lead-free ferroelectric materials with the A<sup>1+</sup>B<sup>5+</sup>O<sub>3</sub> type perovskite structure concerning the environmental friendliness. LT has the rhombohedral crystal structure with crystal symmetry class 3m (unit cell dimensions: a = 5.1530 Å and c = 13.755 Å), large nonlinear constant (d<sub>33</sub> = 13.6 pm/V at 1064 nm), second harmonic generation (SHG) coefficient (d<sub>33</sub><sup>2w</sup> = 40.0 with respect to KDP at 1060 nm) (Risk et al., 2003, JCPDS No. 29-0836, Moses, 1978) and Curie temperature (660°C). In contrast, KN has the orthorhombic crystal structure with crystal symmetry class mm2 (unit cell dimensions: a = 5.6896 Å, b = 3.9693 Å and c = 5.7256 Å), large nonlinear coefficient (d<sub>33</sub> = 27.4 pm/V at 1064 nm) [Moses, 1978] and Curie temperature (435°C). Thus, they exhibit unique electro-optic, piezoelectric, acousto-optic, and nonlinear optical (NLO) properties when doped with rare-earth (RE) [4f<sup>1-13</sup>] elements combined with good mechanical and chemical stability (Abedin et al., 1997, Zhu et al., 1995, Mizuuchi et al., 1995, Zgonik et al., 1993, Xue et al., 1998). Very recently, potassium niobate ceramics were investigated with an aim to develop environmental friendly lead-free piezoelectric and nonlinear materials (Ringgaard & Wurlitzer, 2005).

The electronic structure of each trivalent RE element consists of partially filled 4f subshell, and outer 5s<sup>2</sup> and 5p<sup>6</sup> subshell. With increasing nuclear charge electrons enter into the underlying 4f subshell rather than the external 5d subshell. Since the filled 5s<sup>2</sup> and 5p<sup>6</sup>

subshells screen the 4f electrons, the RE elements have very similar chemical properties. The screening of the partially filled 4f subshells, by the outer closed 5s<sup>2</sup> and 5p<sup>6</sup> subshell, also gives rise to sharp emission spectra independent of the host materials. The intra-subshell transitions of 4f electrons lead to narrow absorption peaks in the ultra-violet, visible, and near-infrared regions.

In this chapter, we report synthesis, structure, properties and application of transparent ferroelectric LiTaO<sub>3</sub> (LT) and KNbO<sub>3</sub> (KN) nanostructured glass-ceramics. They were prepared by controlled volume (bulk) crystallization of their precursor glasses with and without RE dopant. The crystallization processes were studied by differential thermal analysis (DTA), X-ray diffraction (XRD), field emission scanning electron microscopy (FESEM), transmission electron microscopy (TEM), Fourier transform infrared reflection spectra (FT-IRRS), fluorescence and excited state lifetime analyses and dielectric constant measurement. The X-ray diffraction (XRD) patterns, selected area electron diffraction (SAED) and transmission electron microscopic (TEM) images confirm crystallization of LiTaO<sub>3</sub> and KNbO<sub>3</sub> nanocrystals in the transparent glass-ceramics.

## 2. Experimental procedure

### 2.1 Precursor glass and glass-ceramics preparation

The LT precursor glasses having molar composition 25.53Li<sub>2</sub>O-21.53Ta<sub>2</sub>O<sub>5</sub>-35.29SiO<sub>2</sub>-17.65Al<sub>2</sub>O<sub>3</sub> (LTSA) doped with RE ions (0.5 wt% oxides of Eu<sup>3+</sup> and Nd<sup>3+</sup> in excess) or undoped were prepared by the melt-quench technique. The melting of thoroughly-mixed batches was done at 1600°C. The quenched glass blocks were annealed at 600°C for 4 h to remove the internal stresses of the glass and then slowly cooled down (@ 1°C/min) to room temperature. The annealed glass blocks were cut into desired dimensions and optically polished for ceramization and to perform different measurements. The crystallization was carried out at 680°C in between 0-100 h duration.

The KN precursor glasses having composition (mol%) 25K<sub>2</sub>O-25Nb<sub>2</sub>O<sub>5</sub>-50SiO<sub>2</sub> (KNS) doped with Er<sub>2</sub>O<sub>3</sub> (0.5 wt% in excess) or undoped were prepared similarly as mentioned above by the melt-quench technique. The well-mixed raw materials were melted in a platinum crucible in an electric furnace at 1550°C and the quenched glasses were annealed at 600°C to remove the internal stresses of these precursor glasses. They were transformed into nanostructured transparent glass-ceramics by heat-treatment at 800°C in between 0-200 h duration.

### 2.2 Characterization

The density of precursor glasses was measured using Archimedes principle using water as buoyancy liquid. The refractive indices of precursor glass and representative glass-ceramics (d) were measured either on a Pulfrich refractometer (Model PR2, CARL ZEISS, Jena, Germany) at wavelength ( $\lambda_e$  = 546.1 nm) or on a Metricon 2010/M Prism Coupler at different wavelength ( $\lambda$  = 473, 532, 633, 1064 and 1552 nm). Differential thermal analysis (DTA) of precursor glass powder was carried out up to 1000°C at the rate of 10°C/min with a SETARAM TG/DTA 92 or with a Netzsch STA 409 C/CD instrument from room temperature to 900°C at a heating rate of 10°C/min. to ascertain the glass transition temperature ( $T_g$ ) and the crystallization peak temperature ( $T_p$ ). XRD data were recorded

using a PANalytical X'Pert-PRO MPD diffractometer operating with  $\text{CuK}_\alpha = 1.5406 \text{ \AA}$  radiation to identify the developed crystalline phases. The data were collected in the  $2\theta$  range from  $10^\circ$  to  $80^\circ$  with a step size of  $0.05^\circ$ .

A high resolution FE-SEM (Model: Gemini Zeiss Supra™ 35 VP, Carl Zeiss) was used to observe the microstructure of freshly fractured surfaces of the heat-treated nano glass-ceramics after etching in 1% HF solution for 2 minutes and coated with a thin carbon film. The TEM images and selected area electron diffraction (SAED) of powdered glass-ceramic sample were obtained from FEI (Model: Tecnai G<sup>2</sup> 30ST, FEI Company) instrument. The FTIR reflectance spectra of all the glasses and glass-ceramics were recorded using a FTIR spectrometer (Model: 1615, Perkin-Elmer) in the wavenumber range  $400\text{--}2000 \text{ cm}^{-1}$  with a spectral resolution of  $\pm 2 \text{ cm}^{-1}$  and at  $15^\circ$  angle of incidence. Optical absorption spectra were recorded on UV-Vis-NIR spectrophotometer (Model: Lambda 20, Perkin-Elmer) at room temperature. The UV-Vis fluorescence emission and excitation spectra of  $\text{Eu}^{3+}$  doped precursor glass and nano glass-ceramics were measured on a fluorimeter (Model: Fluorolog-II, SPEX) with 150 W Xe lamp as a source of excitation. The fluorescence decay curves were recorded on the same instrument attached with SPEX 1934D phosphorimeter using pulsed Xe lamp. On the other hand, the fluorescence emission and excitation spectra of rest of samples were measured on continuous bench top modular spectrofluorimeter (QuantaMaster, Photon Technology International) attached with gated Hamamatsu NIR PMT (P1.7R) as detector and Xe arc lamp as excitation source. The excited state lifetime was measured with the same instrument using a Xe flash lamp of 75 W. The dielectric constants of precursor glass and nano glass-ceramics were measured at room temperature using a Hioki LCR meter (Model: 3532-50 Hitester, Hioki) at 1 MHz frequency after coating the surfaces with a conductive silver paint followed by drying at  $140^\circ\text{C}$  for 1h. Second harmonic generations (SHG) at 532 nm in the undoped glass-ceramics have been realized under fundamental beam of  $\text{Nd}^{3+}$ :YAG laser source (1064 nm). The input energy of  $\text{Nd}^{3+}$ : YAG laser was fixed at 17 mJ. The input energy of laser was divided in two directions (50% energy in each direction) using reflecting neutral density filter. In one direction KDP was put for reference. The reference SHG signal was measured using photodiode. Second beam was passed through visible filter (which blocks all visible wavelengths but pass 1064 nm) and focused onto the test samples. The SHG generated from the sample was focused onto a second harmonic separator, which reflects 532 nm at  $45^\circ$  and transmit 1064 nm. The SHG signal reflected from SHG separator passed through IR filter was finally measured using PMT. The reference signals from photodiode and from PMT were measured simultaneously using Lecroy oscilloscope (bandwidth 1GHz).

### 3. Nanostructured LiTaO<sub>3</sub> ferroelectric glass-ceramics

#### 3.1 Background

Lithium tantalate (LiTaO<sub>3</sub>, LT) single crystal is one of the most important lead-free ferroelectric materials in the  $\text{A}^{1+}\text{B}^{5+}\text{O}_3$  type perovskite family. The correlation of property alteration of LT single crystals, powders, thin films, glass-ceramics, etc. with processing parameters is an important area of exploration. In recent times researchers have demonstrated the property monitoring based on preparation of LiTaO<sub>3</sub> powders (Zheng et al., 2009) and thin films (Cheng et al., 2005, Youssef et al., 2008) by different methods. Luminescence properties of  $\text{Ho}^{3+}$ ,  $\text{Eu}^{3+}$ ,  $\text{Tb}^{3+}$  etc. doped LiTaO<sub>3</sub> crystals, an another important area of exploration, which have also been investigated by various researchers (Sokólska, 2002, Sokólska et al., 2001, Gasparotto et al., 2008, Gruber et. al., 2006). Rare-earth (RE) doped transparent LiTaO<sub>3</sub> nanocrystallite containing glass ceramics, in which RE ions

selectively incorporated into the  $\text{LiTaO}_3$  nanocrystals embedded in an oxide glassy matrix, can offer excellent luminescent properties due to the low phonon energy environment of  $\text{LiTaO}_3$  nanocrystallites for luminescent ions, and good mechanical and chemical properties of oxide glassy matrix. This ability, combined with inherent nonlinear optical (NLO) properties of ferroelectric crystals, could offer a possibility to design self frequency doubling laser sources. Hence, this new material has attracted great attention in the continuous research for the development of novel optoelectronic devices (Jain, 2004, Romanowski et al., 2000, Hase et al., 1996). Mukherjee and Varma have reported the crystallization and physical properties of  $\text{LiTaO}_3$  in a  $\text{LiBO}_2\text{-Ta}_2\text{O}_5$  reactive glass matrix, however, they have not explored RE doped  $\text{LiTaO}_3$  containing glass-ceramics (Mukherjee & Varma, 2004). As such, work performed on nanocrystalline  $\text{LiTaO}_3$  containing aluminosilicate glass-matrix materials is very rare due to the difficulties in preparation of transparent precursor glass in general and glass-ceramics in particular which involves high temperature (about  $1600^\circ\text{C}$ ) for its precursor glass melting (Ito et al., 1978). For this reason, the structure, dielectric and fluorescence properties of  $\text{Eu}^{3+}$ ,  $\text{Nd}^{3+}$  and  $\text{Er}^{3+}$  ion doped transparent precursor glass and glass-ceramic composites of  $\text{LiTaO}_3$  with heat-treatment time have been studied and reported elaborately by Tarafder et al., 2009 & 2010, Tarafder et al., DOI:10.1111/j.1744-7402.2010.02494.x. Second harmonic generation (SHG) from bulk  $\text{LiTaO}_3$  glass-ceramics has also been studied (Tarafder et al., 2011). For better understanding, the structure, dielectric and fluorescence properties of  $\text{Eu}^{3+}$  and  $\text{Nd}^{3+}$  ion doped transparent precursor glass and glass-ceramic composites of  $\text{LiTaO}_3$  with heat-treatment time have been reported elaborately along with the second harmonic generation (SHG) from bulk  $\text{LiTaO}_3$  glass-ceramics.

## 4. Results and discussion

### 4.1 Differential thermal analysis (DTA)

The DTA curve of the  $\text{Eu}^{3+}$  doped precursor glass is shown in Fig. 1. This exhibits the inflection in the temperature range  $680\text{-}715^\circ\text{C}$  followed by the intense exothermic peak at  $821^\circ\text{C}$  ( $T_p$ ) corresponding to the  $\text{LiTaO}_3$  crystallization. The glass transition temperature ( $T_g$ ) has been estimated to be  $696^\circ\text{C}$  from the point of intersection of the tangents drawn at the slope change as is marked in Fig. 1.

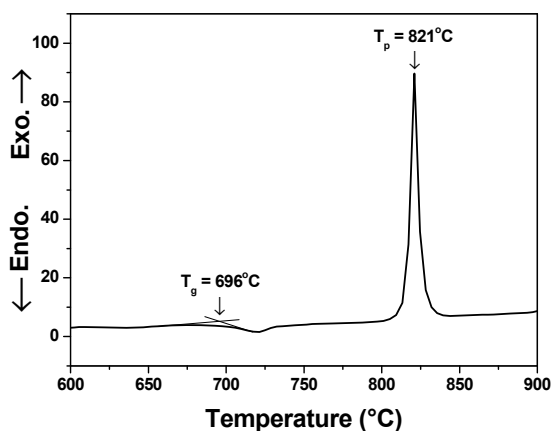


Fig. 1. DTA curve of  $\text{Eu}^{3+}$  doped precursor LTSA powdered glass.

## 4.2 Refractive index

The Eu<sup>3+</sup> doped precursor LTSA glass samples were heat treated at 680°C near glass transition temperature for various heat-treatment durations (0, 1, 3, 5, 7, and 10 h) after nucleating at 650°C for 2 h. Similarly, the Nd<sup>3+</sup> doped precursor LTSA glass samples were heat treated at 680°C for 0, 3, 5, 10, 20, 50 and 100 h and were labeled as a, b, c, d, e, f and g. The Nd<sup>3+</sup> doped precursor glass and nano glass-ceramics are presented in Fig. 2. From the measured glass density ( $\rho$ ) and refractive index ( $n_e$ ) at wavelength  $\lambda_e = 546.1$  nm, other related optical properties of Eu<sup>3+</sup> doped precursor glass have been determined using relevant expressions and the same is presented in Table 1. Fig. 3 present Cauchy fitting based on measured refractive indices at five different wavelengths (see experimental procedure) and shows the dependences of the refractive index on the wavelength for Nd<sup>3+</sup> doped precursor glass (a) and representative heat-treated glass-ceramics samples. In general, refractive index decreases with increasing wavelength due to dispersion. In addition to this, the refractive index of the glass-ceramics samples has increased in comparison with precursor glass (a) that can be seen in Fig. 3. The refractive indices  $n_F$ ,  $n_D$  and  $n_C$  have been estimated at three standard wavelengths ( $\lambda_F = 486.1$  nm,  $\lambda_D = 589.2$  nm and  $\lambda_C = 656.3$  nm respectively) from the dispersion curve (Figs. 3, curve a). Similarly, from the measured glass density ( $\rho$ ) and refractive index ( $n_D$ ) at wavelength  $\lambda_D = 589.2$  nm, other related optical properties of Nd<sup>3+</sup> doped precursor glass have also been determined and the results are presented in Table 1. From Table 1, it is clear that the LTSA glass under study has high values of refractive index and density. The large refractive indices of this glass are due to high ionic refraction (23.4) of Ta<sup>5+</sup> ions (Volf, 1984) having an empty or unfilled d-orbital (outer electronic configuration: 5d<sup>0</sup>6s<sup>0</sup>) which contributes strongly to the linear and nonlinear polarizability (Yamane & Asahara, 2000). The high density of the glass has originated from the large packing effect of Ta in the glass matrix (Hirayama & Berg, 1963). For the same reason, this glass possesses a high value of molar refractivity and electronic polarizability. Due to formation of high refractive index LiTaO<sub>3</sub> (RI = 2.1834 at 600 nm (Lynch, 1975)), the heat-treated sample exhibit higher refractive indices as shown in Fig. 3, curve-d.

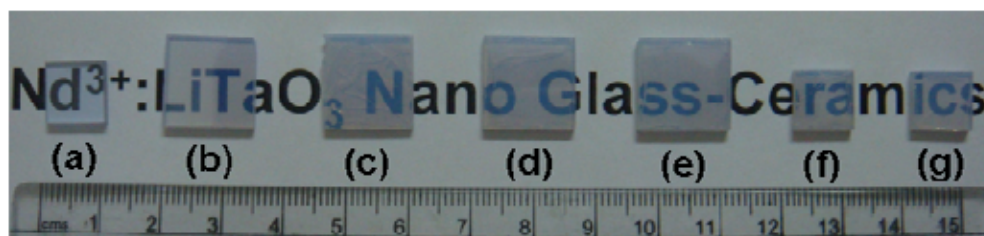


Fig. 2. (Color online) Photographs of Nd<sup>3+</sup> doped precursor LTSA glass and LT nano glass-ceramics (thickness: 2 mm) laid over the writing to show their transparency respectively.

## 4.3 X-ray diffraction analysis

The X-ray diffractogram of Eu<sup>3+</sup> doped precursor LTSA glass and cerammed glass-ceramics are shown in Fig. 4. The XRD pattern of the precursor glass exhibits broad humps characterizing its amorphous structure. With progression of heat-treatment, several diffraction peaks have been appeared in the glass-ceramics. From the analysis of these peaks it has been concluded that these peaks are attributed to rhombohedral LiTaO<sub>3</sub> (JCPDS Card

Properties	Corresponding value	
	Eu <sup>3+</sup> :LiTaO <sub>3</sub> doped precursor glass	Nd <sup>3+</sup> :LiTaO <sub>3</sub> doped precursor glass
Average molecular weight, $M_{av}$	142.47	142.37
Density, $\rho$ (g.cm <sup>-3</sup> )	4.54	4.50
Refractive index	$n_e$ (at 546.1 nm) $\rightarrow$ 1.7852	$n_F$ (at 486.1 nm) $\rightarrow$ 1.8053 $n_D$ (at 589.2 nm) $\rightarrow$ 1.7894 $n_C$ (at 656.3 nm) $\rightarrow$ 1.7821
Molar refractivity, $R_M$ (cm <sup>3</sup> )	13.23	13.39
Electronic polarizability, $\alpha$ (cm <sup>3</sup> )	$1.84 \times 10^{-21}$	$1.79 \times 10^{-21}$
RE <sup>3+</sup> ion concentration, $N_{RE^{3+}}$ (ions/cm <sup>3</sup> )	$5.71 \times 10^{19}$	$5.66 \times 10^{19}$
Glass transition temperature, $T_g$ (°C)	696	702
Crystallization peak, $T_p$ (°C)	821	820

Table 1. Some measured and calculated properties of RE<sup>3+</sup>:LiTaO<sub>3</sub> precursor glass

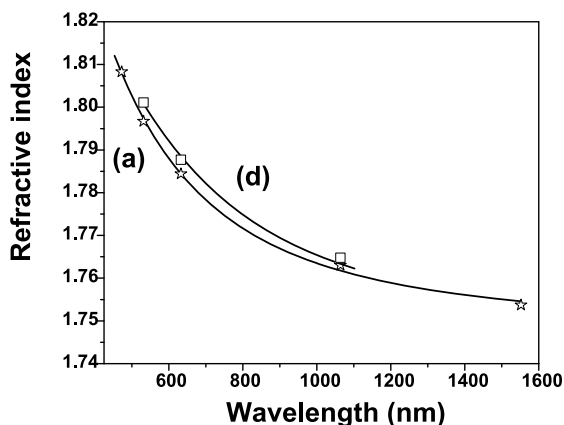


Fig. 3. Variation of refractive indices (Cauchy fitted) of Nd<sup>3+</sup> doped (a) precursor LTSA glass and (d) 10 h heat-treated LT nano glass-ceramic as a function of wavelength.

File No. 29-0836) except a few diffraction peak around  $2\theta = 23.0^\circ$ ,  $25.5^\circ$ ,  $44.5^\circ$  and  $47.0^\circ$  which are due to the formation of  $\beta$ -spodumene (LiAlSi<sub>2</sub>O<sub>6</sub>) crystal phase (JCPDS Card File No. 35-0797) in minor quantity. It is clearly evidenced from the XRD analysis that the peak of LiAlSi<sub>2</sub>O<sub>6</sub> ( $2\theta = 25.5^\circ$ ) is more prominent in sample of 5 h heat-treatment and it got diminished with respect to LiTaO<sub>3</sub> phase in longer heat-treated glass-ceramics, indicating the stabilization of LiTaO<sub>3</sub> nanocrystallites with increase in heat-treatment duration. From the full width at half maximum (FWHM) of the most intense diffraction peak (012) of

LiTaO<sub>3</sub>, the average crystallite size (diameter, *d*) is calculated by using the Scherrer's formula (Cullity, 1978)

$$d = 0.9\lambda / \beta \cos \theta \quad (1)$$

where  $\lambda$  is the wavelength of X-ray radiation ( $\text{CuK}\alpha = 1.5406\text{\AA}$ ),  $\beta$  is the full width at half maximum (FWHM) of the peak at  $2\theta$ . The average crystallite size of each RE doped heat-treated glass-ceramics found to increase with heat-treatment duration.

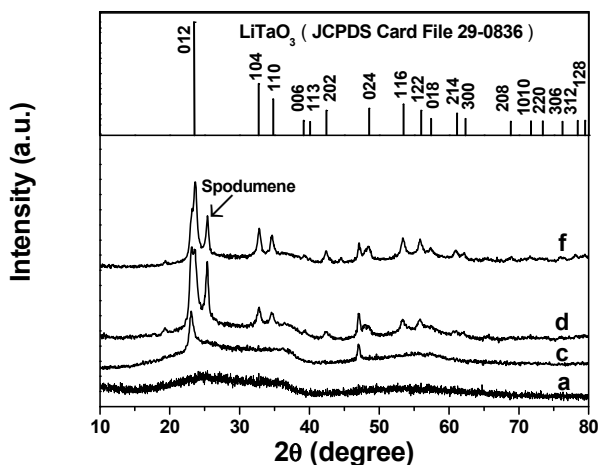


Fig. 4. XRD pattern of Eu<sup>3+</sup> doped precursor powdered LTSA glass and LT nano glass-ceramics.

#### 4.4 FESEM and TEM image analyses

The morphology and LiTaO<sub>3</sub> crystallite size of Eu<sup>3+</sup> and Nd<sup>3+</sup> doped nano glass-ceramics have been examined by FESEM and TEM image analyses. FESEM images of the fractured surface of Nd<sup>3+</sup> doped nano glass-ceramics have been presented in Figs. 5(a)-(b). The Nd<sup>3+</sup> doped glass-ceramics 5(a) is obtained by heat-treating the precursor glasses at 680°C for 5 h. Similarly, the glass-ceramics 5(b) is obtained by heat-treating the precursor glasses at 680°C for 20 h. From the FESEM micrographs, it is clearly observed that the glassy matrix of the heat-treated samples initially phase separated on nanometric scale followed by incipient precipitation of defined crystallites within the Li-Ta rich phase regions with increase in heat-treatment time. The droplets have irregular shapes and dispersed uniformly throughout the bulk glass matrix. The size of the droplets varies in the range 20-60 nm. TEM image of the Eu<sup>3+</sup> doped 10 h heat-treated glass-ceramics (f) has been presented in Fig. 6(a). The SAED pattern of the observed crystalline phase is presented in Fig. 6(b). From this image, it is observed that many spheroidal LiTaO<sub>3</sub> crystallites precipitated homogeneously from the glass matrix and remained homogeneously dispersed in the residual glass matrix. The crystallite size from this TEM image of sample f found to be around 18 nm. The presence of fine spherical rings around the central bright region in SAED pattern discloses the existence of LiTaO<sub>3</sub> nanocrystallites in the glassy matrix.

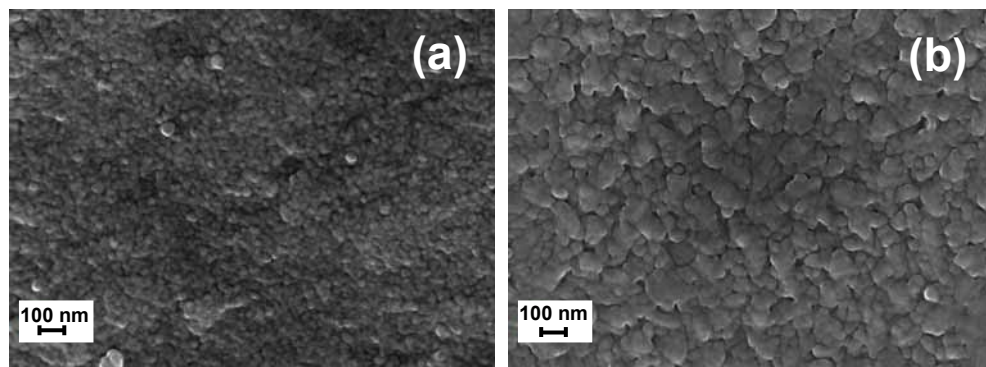


Fig. 5. FESEM image of  $\text{Nd}^{3+}$  doped samples (a) c and (b) e.

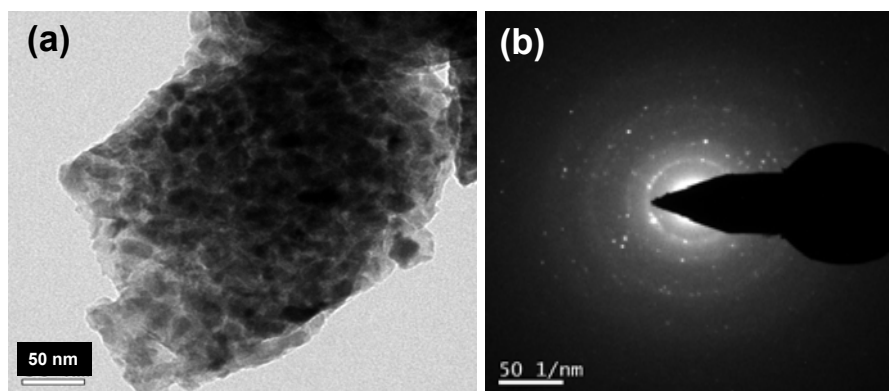


Fig. 6. (a) TEM image and (b) SAED pattern of  $\text{Eu}^{3+}$  doped glass-ceramics sample f.

#### 4.5 Fourier transform infrared reflectance spectroscopy (FTIRRS)

The FTIR reflectance spectra of the  $\text{Nd}^{3+}$  doped precursor LTSA glass and heat-treated glass-ceramic samples in the wavenumber range  $400\text{--}2000\text{ cm}^{-1}$  is shown in Fig. 7. It is seen from this figure that the precursor glass (curve-a) exhibits two broad reflection bands centered around  $960$  and  $610\text{ cm}^{-1}$  as a result of wider distribution of silicon and tantalate structural units respectively. As alumina is one of the glass constituents, it prefers to enter into the silica rich phase and somewhere replace the  $\text{Si}^{4+}$  and the charge is compensated by  $\text{Li}^{+}$  ion. But, in order to maintain neutral charge condition, the later phase contains a higher amount of  $\text{Li}^{+}$  ions as the  $\text{TaO}_6$  octahedra are negatively charged (Fukumi & Sakka, 1988, Samuneva et al., 1991). Hence, from the rearrangement of the glassy matrix it can be indicated that both the phase separated compositions begin to crystallize producing a nanostructure with the prolonged heat-treatment time. The appearance of a low intensity band at  $735\text{ cm}^{-1}$  upon heat-treatment related to the stretching mode of Al-O bond of  $\text{AlO}_4$  tetrahedra of  $\beta$ -spodumene (Burdick & Day, 1967). The prominent band occurred at  $600\text{ cm}^{-1}$  corresponds to the stretching mode of O-Ta bond of  $\text{TaO}_6$  octahedral units of lithium tantalate (Ono et al., 2001, Zhang et al., 1999). The reflection band centered at  $600\text{ cm}^{-1}$  is assigned as  $\text{LiTaO}_3$  crystal formation and the reflection band centered at  $1000\text{ cm}^{-1}$  is assigned to Si-O stretching

vibration of residual glass and  $\beta$ -spodumene crystal. The variation of Si-O (998 cm<sup>-1</sup>) and Ta-O (602 cm<sup>-1</sup>) stretching vibration bands intensities (here reflectivity) of Nd<sup>3+</sup> doped samples with heat-treatment time is also recorded. It is seen that with progression of heat-treatment the band intensities increase rapidly initially and then become almost saturated after a certain time of heat-treatment (10 h). The gradual increase of relative intensity of band at 600 cm<sup>-1</sup> clearly indicates formation of LiTaO<sub>3</sub> crystal with the increase of heat treatment time. The results of the FT-IRRS are in good agreement with that of XRD, FE-SEM and TEM studies. A similar observation has also been reported by Ito et al., 1978.

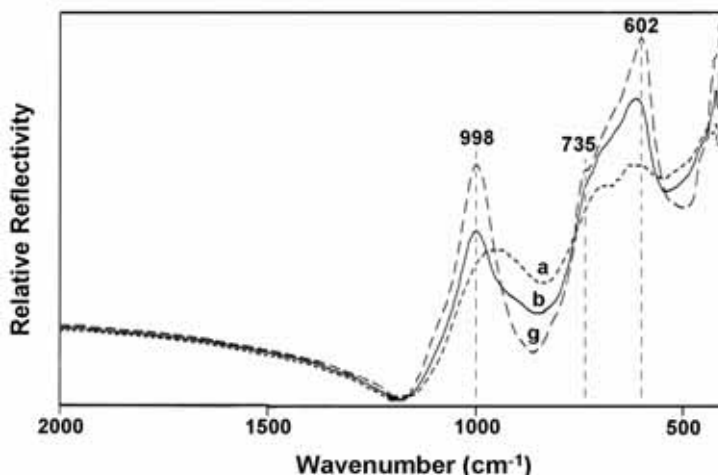


Fig. 7. FTIR-RS spectra of Nd<sup>3+</sup> doped precursor LTSA glass and LT nano glass-ceramics.

#### 4.6 Dielectric constant ( $\epsilon_r$ )

The as prepared Eu<sup>3+</sup> and Nd<sup>3+</sup> doped LTSA precursor glasses exhibit relatively higher value ( $\sim 20.0$ ) of dielectric constant ( $\epsilon_r$ ) than the common vitreous silica (3.8) or soda-lime silicate (7.2) or borosilicate glasses (4.1-4.9) (Blech, 1986) due to high ionic refraction of Ta<sup>5+</sup> ions (23.4) (Volf, 1984). This is due to its empty or unfilled d-orbital which contributes very strongly to its high polarizability (Yamane & Asahara, 2000, Risk et al., 2003). Its magnitudes show a sharp increase with increase in heat-treatment duration up to 5 h and thereafter it maintained saturation with a small decrease for any further heat treatment time as shown in Fig. 8. This suggests that, at the initial stages of heat treatment (1-3 h), separation of silica rich phase and Li-Ta enriched phases takes place and with the further heat-treatment, incipient precipitation of LiTaO<sub>3</sub> crystalline phase of high dielectric constant ( $\epsilon_r = 52$ ) (Moses, 1978) and spontaneous polarization ( $P_s = 0.50$  C/m<sup>2</sup>) (Risk et al., 2003) occurs gradually which becomes well defined at 5 h and attains the maximum volume fraction of the crystalline phase. Thus accumulation of Li<sup>+</sup> ions in the phase-separated glass matrix initially could cause a slight increase of dielectric constant and with further heat treatment time due to formation of stable LiTaO<sub>3</sub> ferroelectric crystals remarkably increase the dielectric constant reaching the highest value for 5 h heat treated sample and then maintain almost same on further course of heat-treatment. The variation in the dielectric constant ( $\epsilon_r$ ) values among the heat-treated nano glass-ceramics are mostly due to volume fraction of crystal

phases contained and also the distribution of the  $\text{LiTaO}_3$  phase in the microstructure (Vernacotola, 1994).

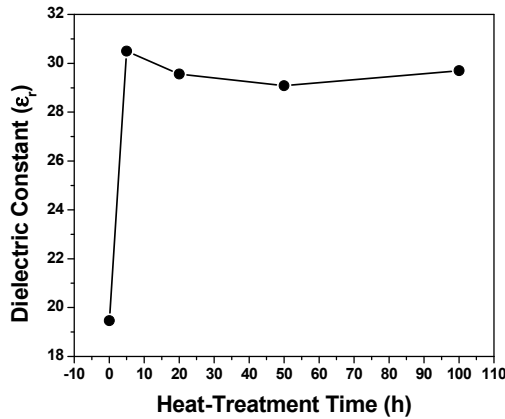


Fig. 8. Variation of dielectric constant of  $\text{Nd}^{3+}$  doped precursor LTSA glass and LT nano glass-ceramics as a function of heat-treatment time.

#### 4.7 UV-Visible-NIR absorption spectra

The room temperature measured absorption spectra of the  $\text{Nd}^{3+}$  doped precursor glass (a) and 100 h heat-treated glass-ceramic samples (g) in the visible-NIR range have been presented in Fig. 9. The spectra reveal absorption peaks due to the  $4f^3-4f^3$  forced electric dipole transitions from the ground  $^4I_{9/2}$  state to different excited states of  $\text{Nd}^{3+}$  ion in  $4f^3$  configuration. All the peaks  $^4I_{9/2} \rightarrow ^4G_{9/2}$  (512 nm),  $^2K_{13/2} + ^4G_{7/2} + ^4G_{9/2}$  (526 nm),  $^4G_{5/2} + ^2G_{7/2}$  (583 nm),  $^2H_{11/2}$  (626 nm),  $^4F_{9/2}$  (679 nm),  $^4F_{7/2} + ^4S_{3/2}$  (739 nm),  $^4F_{5/2} + ^2H_{9/2}$  (806 nm) and  $^4F_{3/2}$

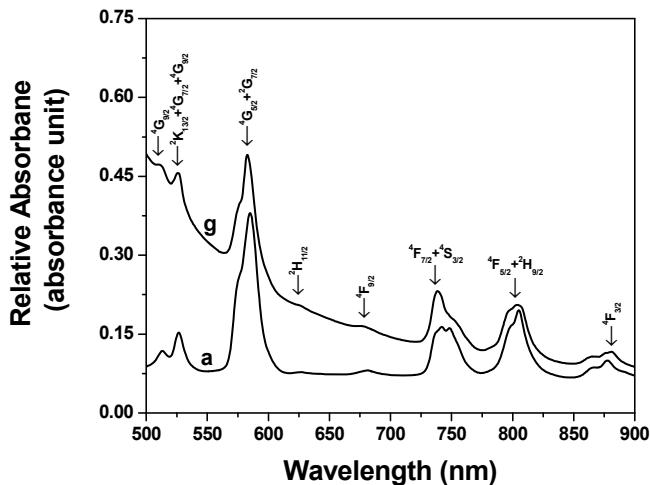


Fig. 9. Absorption spectra of  $\text{Nd}^{3+}$  doped samples (a) and (g) (thickness: 2 mm).

(880 nm) are assigned in accordance with Carnall's convention (Carnall et al., 1968, Chen et al., 2005). From this figure it is noticed that the base line of absorption spectra of heat-treated sample (g) has been elevated significantly with the diminished intensity of the absorption peak. This uplifting can be attributed to scattering of short wavelength light by the crystals (Beall & Duke, 1983 & 1969] or may be due to the difference in refractive index of crystalline phase (RI of LiTaO<sub>3</sub> is 2.1834 at 600 nm (Lynch, 1975)) with that of residual glassy matrix.

#### 4.8 Photoluminescence spectra

The photoluminescence emission spectra of precursor glass (a) and Eu<sup>3+</sup>:LiTaO<sub>3</sub> containing nano glass-ceramics (c and f) are recorded with an excitation at 392 nm and depicted in Fig. 10(A). All the spectra exhibit emissions from <sup>5</sup>D<sub>0</sub> excited level to the ground state multiplets <sup>7</sup>F<sub>0, 1, 2, 3, 4</sub> levels of Eu<sup>3+</sup> ions with overall dominance of electric dipole (ED) transition <sup>5</sup>D<sub>0</sub>→<sup>7</sup>F<sub>2</sub>. The emission peak around 532 nm has been assigned to <sup>5</sup>D<sub>1</sub>→<sup>7</sup>F<sub>2</sub> transition. In the perovskite type LiTaO<sub>3</sub> crystals, Li<sup>+</sup> and Ta<sup>5+</sup> occupy octahedral sites with C<sub>3</sub> or nearly C<sub>3v</sub> point symmetry. The Eu<sup>3+</sup> ion is entering into the crystal (LiTaO<sub>3</sub>) and it prefers to replace Li<sup>+</sup> over Ta<sup>5+</sup> site forming [REO<sub>6</sub>]<sup>9-</sup> octahedron (Wu & Zheng, 2002, Wu & Dong, 2005, Chang et al., 1993) due to the closeness of their ionic radii (Eu<sup>3+</sup> = 0.95 Å, Li<sup>+</sup> = 0.74 Å and Ta<sup>5+</sup> = 0.64 Å). The local field asymmetry defining factor such as relative intensity ratio of I<sub>ED</sub> to I<sub>MD</sub> of Eu<sup>3+</sup> doped glass and nano glass-ceramics has been estimated from their photoluminescence spectra and it was found that the asymmetric ratio of all samples was greater than unity, which implies that the Eu<sup>3+</sup> ions take non-centrosymmetric sites.

The infrared photoluminescence spectra (λ<sub>ex</sub> = 809 nm) of the Nd<sup>3+</sup> doped samples (a, c and g) around 1069 nm are shown in Fig. 10(B). The emission band intensity around 1069 nm decreases with progression of heat-treatment. This decrease in emission intensity is due to the clustering of Nd<sup>3+</sup> ions which is extremely sensitive to concentration quenching (Riello et al., 2006). Dejneka, 1998, has demonstrated in fluoride glasses that clustering thereby quenching occurs when the Eu<sup>3+</sup>-Eu<sup>3+</sup> ionic separation is around 40 Å. In the present case, the Nd<sup>3+</sup>-Nd<sup>3+</sup> ionic separation (R<sub>i</sub>) in the precursor glass is found to be about 26 Å which was calculated using the relation (Pátek, 1970):

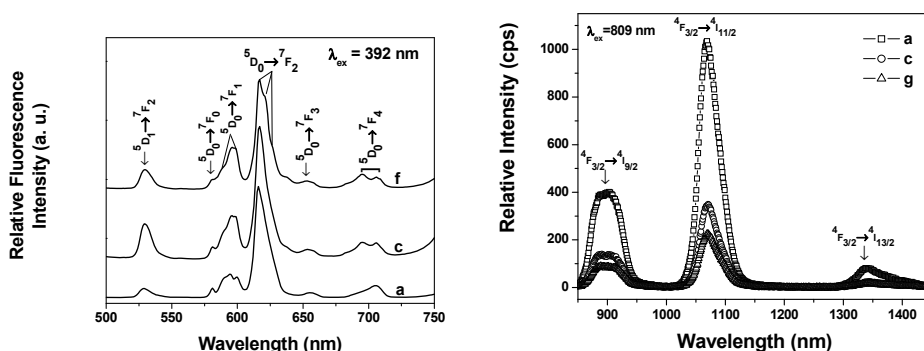


Fig. 10. Photoluminescence spectra of (A) Eu<sup>3+</sup> and (B) Nd<sup>3+</sup> doped precursor LTSA glass and LT nano glass-ceramics (thickness: 2 mm) respectively.

$$R_i(\text{\AA}) = (1 / N_{\text{Nd}^{3+}})^{1/3} \quad (2)$$

where  $N_{\text{Nd}^{3+}}$  is the  $\text{Nd}^{3+}$  ion concentration. It is, therefore, seen that the  $\text{Nd}^{3+}$ -  $\text{Nd}^{3+}$  ionic separations ( $R_i$ ) are in the quenching region. Theoretically, the rate of relaxation due to concentration quenching varies as  $R_i^{-6}$  (Campbell & Suratwala, 2000, Kang et al., 2001, Zgonik et al., 1993). With the progression of heat-treatment, the  $\text{LiTaO}_3$  crystal phase has been formed and the  $\text{Nd}^{3+}$  ions partitioned into the residual glassy phase by reducing the inter-ionic separation less than 40 Å. This fact results in reduction in fluorescence intensity due to concentration quenching. The emission bands become sharper and take shapes as in crystalline host with progress of heat-treatment duration. All these observations indicate that the  $\text{Nd}^{3+}$  ions enter into the  $\text{LiTaO}_3$  crystalline phase and therefore, environment around  $\text{Nd}^{3+}$  ions is changed with progression of heat-treatment.

#### 4.9 Second harmonic generation (SHG)

The variation of SHG output power (nJ) with time period in bulk LTSA glass and LT glass-ceramics has been shown in Figs. 11(a) and (b). It is seen from the Fig. 11(a) that the precursor LTSA glass does not exhibit any SHG output. This is due to inversion symmetry of the precursor glass. It is also observed that for a constant heat-treatment time (10 h), the SHG output power increase from 1.08 to 1.875 nJ when the temperature is increased from 680°C to 850°C. This is attributed due to the formation of ferroelectric (non-centrosymmetric)  $\text{LiTaO}_3$  crystals in the glassy matrix. Moreover, the increase in SHG output power with subsequent increase of heat-treatment temperature is due to the increase of  $\text{LiTaO}_3$  crystallites content and their sizes in the glassy matrix.

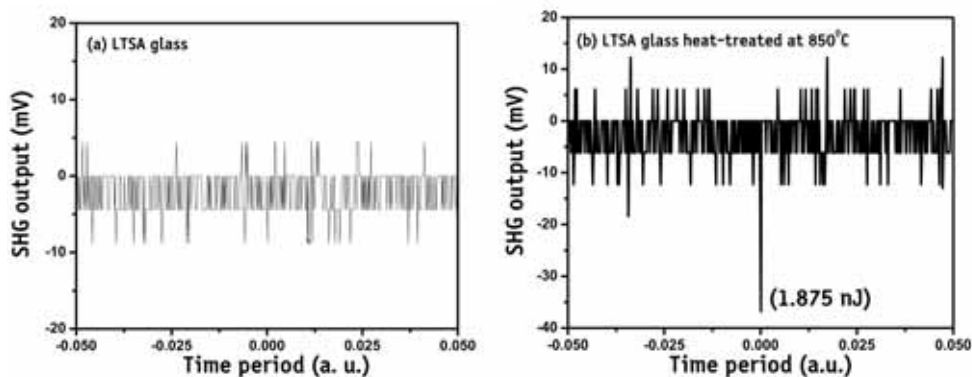


Fig. 11. Variation of SHG output power (nJ) with time period of precursor (a) LTSA glass and (b) 850°C heat-treated for 10 h LT glass-ceramic sample.

## 5. Nanostructured $\text{KNbO}_3$ ferroelectric glass-ceramics

### 5.1 Background

Ferroelectric potassium niobate ( $\text{KNbO}_3$ , KN) has the  $\text{A}^{1+}\text{B}^{5+}\text{O}_3$  perovskite-type (orthorhombic) crystal structure (crystal symmetry class  $mm2$ ; unit cell dimensions:  $a = 5.6896$  Å,  $b = 3.9693$  Å and  $c = 5.7256$  Å) and having large nonlinear coefficient ( $d_{33} = 27.4$

pm/V at 1064 nm). It is widely used in frequency doubling, tunable wave guiding, active laser host, holographic storage and surface acoustic wave (Xue & Zhang, 1998, Zgonik et al., 1993, Risk et al., 2003). Consequently, it becomes a subject of intense study. Very recently, potassium niobate ceramics were revisited in the interest of a search for environmental friendly lead-free piezoelectric and nonlinear materials (Ringgaard & Wurlitzer, 2005). Due to the low cost and high speed fabrication process of glass technology in comparison to single crystal preparation, with the flexibility of tailored properties to produce transparent nanostructures by controlled crystallization, ferroelectric KNbO<sub>3</sub> containing transparent glass-ceramics have generated increasing academic and technological interests. A large electro-optic effect ( $r_{42} = 380$  pm/V for KNbO<sub>3</sub> (Ringgaard & Wurlitzer, 2005)) has been observed in a number of transparent glass-ceramic materials containing a ferroelectric crystalline phase. Several isothermal or non-isothermal studies have been carried out with a view to generate KNbO<sub>3</sub>, KNbSi<sub>2</sub>O<sub>7</sub>, K<sub>3</sub>Nb<sub>3</sub>Si<sub>2</sub>O<sub>13</sub> etc. ferroelectric crystal phases in various compositions of the K<sub>2</sub>O-Nb<sub>2</sub>O<sub>5</sub>-SiO<sub>2</sub> (KNS) glass system (Pernice et al., 1999 & 2000, Golubkov et al., 2001, Tanaka et al., 2003, Aronne et al., 2004) and noticed strong second harmonic generation (SHG). It is observed that these glass-ceramics doped with rare earth (RE) ions, become very good luminescent media which are able to generate and amplify light. This application in combination with inherent nonlinear optical (NLO) properties of ferroelectric crystals, could offer a possibility to design self frequency doubling laser sources (Ringgaard, & Wurlitzer, 2005). For these reasons, the structure, dielectric and fluorescence properties of Eu<sup>3+</sup>, Nd<sup>3+</sup> and Er<sup>3+</sup> ion doped transparent precursor glass and glass-ceramic composites of KNbO<sub>3</sub> with heat-treatment time have been studied and reported elaborately by Chaliha et al., 2009 & 2010. Second harmonic generation (SHG) from bulk KNbO<sub>3</sub> glass-ceramics has also been studied by Tarafder et al., 2011. For better understanding, the structure, dielectric and fluorescence properties of Er<sup>3+</sup> doped transparent precursor glass and glass-ceramic composites of KNbO<sub>3</sub> with heat-treatment time have been reported elaborately along with the second harmonic generation (SHG) from bulk KNbO<sub>3</sub> glass-ceramics.

In comparison to the other rare earth ions, Er<sup>3+</sup> has been extensively used as the most suitable active ion in several hosts by normal fluorescence for optical amplification at 1.5  $\mu$ m. Trivalent erbium ions characterized by the  $^4I_{13/2} \rightarrow ^4I_{15/2}$  intra-4f transition play the key role in near infrared (NIR) emission (Dai et al., 2005). Besides, Er<sup>3+</sup> doped glasses are chosen for getting better lasing property that can act as an eye-safe laser sources near 1550 nm. The photoluminescent emission intensity of erbium doped glasses is mainly dependent on the chemical environment of Er<sup>3+</sup> ion because in the excited state Er<sup>3+</sup> ion can de-excite by either photon emission at 1.53  $\mu$ m, or non-radiative relaxation through coupling to a quenching site. Also, if the symmetry of the local crystal field around the erbium ion in the host glass is not distorted, the emission of erbium ion is forbidden. Therefore, the erbium ions must be incorporated in a non-centrosymmetric host material for strong optical emission (Winburn, 1985, Hui et al., 2007). Similarly, under favorable conditions strong green emission at 551 nm is possible upon normal high energy excitation.

## 6. Results and discussion

### 6.1 Differential thermal analysis (DTA)

The DTA curve of the Er<sup>3+</sup> doped precursor glass is shown in Fig. 12. It exhibit the inflection in the temperature range 647-689°C followed by the intense exothermic peak at 759°C ( $T_p$ ) corresponding to the phase crystallization. The glass transition temperature ( $T_g$ ) has been

estimated to be 681°C from the point of intersection of the tangents drawn at the slope change as is marked in Fig. 12.

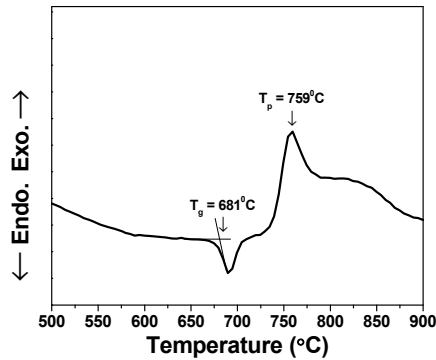


Fig. 12. DTA curve of  $\text{Er}^{3+}$  doped precursor powdered KNS glass.

## 6.2 Refractive index

The precursor glass was heat-treated at 800°C near glass transition temperature for various heat-treatment durations after nucleating at 750°C for 2 h. The prepared glass was transparent with body color of pink. From the measured glass density ( $\rho$ ) and refractive index ( $n_e$ ) at wavelength  $\lambda_e = 546.1$  nm, other related optical properties of  $\text{Er}^{3+}$  doped precursor glass have been determined using relevant expressions and the same is presented in Table 2. The refractive indices of glass and heat-treated samples at five different wavelengths (473, 532, 633, 1064 and 1552 nm) are shown in Fig. 13. It is seen that the refractive index of 100 h heat-treated sample is higher as compared to the precursor glass. This is due to the formation of  $\text{KNbO}_3$  crystals having high refractive index (2.2912 at 600 nm (Palik, 1998)). The large refractive index of this glass is due to the presence of highly

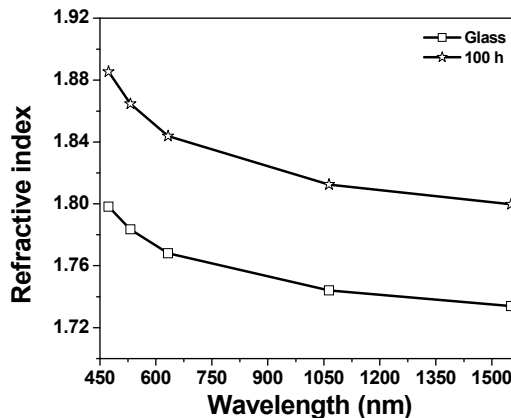


Fig. 13. Variation of refractive indices of precursor KNS glass and KN glass-ceramics obtained after heat-treatment for 100 h as a function of wavelength.

polarizable Nb<sup>5+</sup> ions with high ionic refraction, 24.5 (Volf, 1984). It is observed that ions with an empty or unfilled d-orbital such as Nb<sup>5+</sup> ion (outer electronic configuration: 4d<sup>0</sup>5s<sup>0</sup>) contributes very strongly to the linear and nonlinear polarizabilities (Yamane & Asahara, 2000). For the same reason, this glass is also possessing a high value of molar refractivity ( $R_M = 14.95 \text{ cm}^3$ ) and electronic polarizability ( $\alpha = 5.592 \times 10^{-24} \text{ cm}^3$ ) (Vernacotola & Shelby, 1994).

Properties	Corresponding value
	Er <sup>3+</sup> :KNbO <sub>3</sub> doped precursor glass
Average molecular weight, $M_{av}$	120.05
Density, $\rho$ (g.cm <sup>-3</sup> )	3.37
Refractive index	$n_e$ (at 546.1 nm) $\rightarrow$ 1.78076 $n_F'$ (at 480.0 nm) $\rightarrow$ 1.79612 $n_C'$ (at 643.8 nm) $\rightarrow$ 1.76688
Molar refractivity, $R_M$ (cm <sup>3</sup> )	14.95
Electronic polarizability, $\alpha$ (cm <sup>3</sup> )	$5.592 \times 10^{-24}$
RE <sup>3+</sup> ion concentration, $N_{RE^{3+}}$ (ions/cm <sup>3</sup> )	$5.41 \times 10^{19}$
Glass transition temperature, $T_g$ (°C)	681
Crystallization peak, $T_p$ (°C)	759

Table 2. Some measured and calculated properties of Er<sup>3+</sup>:KNbO<sub>3</sub> precursor glass

### 6.3 X-ray diffraction analysis

Fig. 14 shows the X-ray diffractogram of precursor glass along with the glass-ceramic samples. The amorphous nature of the as-prepared glass is indicated by the XRD pattern consisting of only a broad and halo band at around 29° diffraction angle. The structuring of this halo band takes place in the XRD pattern of the heat-treated glass-ceramic samples of 1-100 h along with the appearance of other well defined peaks around 25°, 28.5°, 30°, 32.8° and

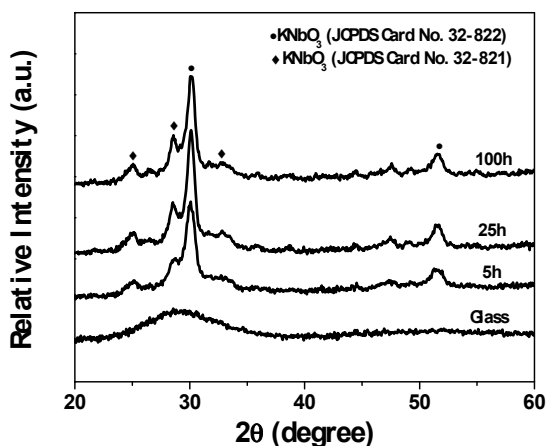


Fig. 14. XRD pattern of precursor KNS glass and glasses heat-treated at 800°C for different duration.

51.5° diffraction angles, which confirms the precipitation crystalline phase in the amorphous matrix. The crystalline phase resembles the JCPDS cards 32-821 and 32-822 of known potassium niobate. The calculated average crystallite sizes lie in the range 5-12 nm.

#### 6.4 FESEM and TEM image analyses

The FESEM photomicrographs of the sample heat-treated at 800°C for 3 and 50 h duration are taken and from the FESEM micrographs, it is clearly observed that the glassy matrix of the heat-treated samples initially phase separated on nanometric scale followed by incipient precipitation of defined crystallites within the Nb-K rich phase regions on prolonged heat-treatments. The TEM image and SAED pattern of the sample heat treated for 50 h at 800°C have been presented in Figs. 15(a) and 15(b) respectively. The crystallite size from this TEM image of 50 h heat-treated sample found to be around 20 nm. The presence of fine spherical rings around the central bright region in SAED pattern discloses the existence of  $\text{KNbO}_3$  nanocrystallites in the glassy matrix.

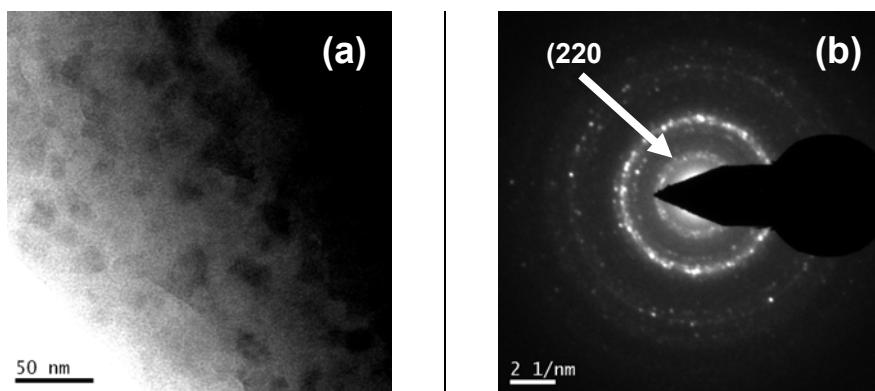


Fig. 15. (a) TEM image and (b) SAED pattern of  $\text{Eu}^{3+}$  doped 50 h heat-treated sample.

#### 6.5 Fourier transform infrared reflectance spectroscopy (FTIRRS)

Fig. 16 shows the comparative FTIR reflectance spectra (FTIRRS) of the precursor glass and samples heat-treated at 800°C for 2 and 100 h duration in the wavenumber range 500-2000  $\text{cm}^{-1}$ . Its inset shows the reflectivity at 930 and 749  $\text{cm}^{-1}$  of precursor glass and heat-treated glasses as a function of heat-treatment time. It is seen that the FTIR spectrum of the precursor glass exhibits a broad reflection band centered at 930  $\text{cm}^{-1}$  as a result of wider distribution of  $\text{SiO}_4$  structural units. The FTIR reflectance spectra of 2 and 100 h reveal narrowing of the main reflection band with additional features arising at 1128, 749 and 598  $\text{cm}^{-1}$  in comparison to the precursor glass (Pernice et al., 1999). In the FTIR spectra, the stretching modes of the Si-O-Si bonds of the  $\text{SiO}_4$  tetrahedra with nonbridging oxygen (NBO) atoms are active in 900-1000  $\text{cm}^{-1}$  range and the stretching modes of the Nb-O bonds in the  $\text{NbO}_6$  octahedra occur in the 700-800  $\text{cm}^{-1}$  range (Samuneva et al., 1991). The reflection band at 1128  $\text{cm}^{-1}$  and 930  $\text{cm}^{-1}$  wavenumber can be related to the asymmetric and symmetric stretching vibration modes of Si-O bonds in  $\text{SiO}_4$  tetrahedra respectively, while the band at 749  $\text{cm}^{-1}$  is due to the Nb-O stretching modes of distorted  $\text{NbO}_6$  octahedra (de Andrade et al., 2000, Silva et al., 2006). The band observed around 598  $\text{cm}^{-1}$  is assigned as  $\nu_2$  bending vibrational modes of the Si-O bonds in the  $\text{SiO}_4$  tetrahedra.

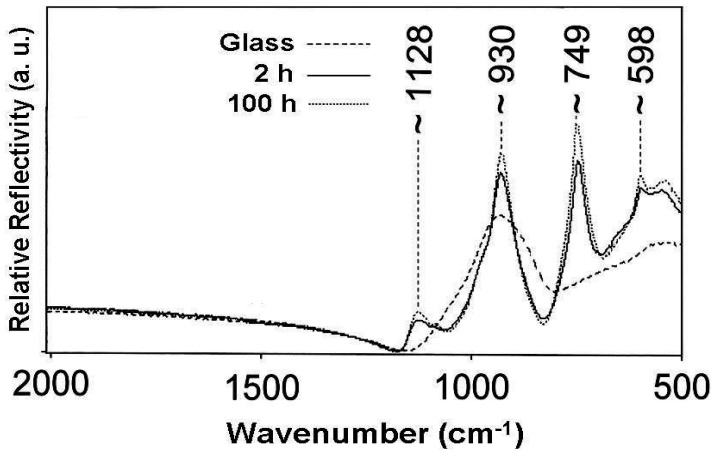


Fig. 16. FTIR-RS spectra of Er<sup>3+</sup> doped precursor KNS glass and KN nano glass-ceramics.

### 6.6 Dielectric constant ( $\epsilon_r$ )

Fig. 17 shows the magnitude of dielectric constant of precursor glass and heat-treated glass-ceramics. From this Fig., it is observed that the dielectric constant increase steeply from  $\epsilon_r = 17$  (for precursor glass) to  $\epsilon_r = 31$  (for 100 h heat-treated glass-ceramics) and thereafter it maintains almost saturation for any further heat treatment time. This suggests that on heat-treatment, at the initial stages, separation of silica rich phase and K-Nb enriched phases takes place and with the further prolonged heat-treatments incipient precipitation of KNbO<sub>3</sub> having high dielectric constant ( $\epsilon_r = 137$ ) (Simões et al., 2004) and spontaneous polarization,  $P_s = 0.41$  C/m<sup>2</sup> (Risk et al., 2003). The variation in crystallite size distributions and also the distribution of the KNbO<sub>3</sub> phase in the microstructure are the causes for the differences in the dielectric constant values amongst the heat-treated samples (Vernacotola, 1994).

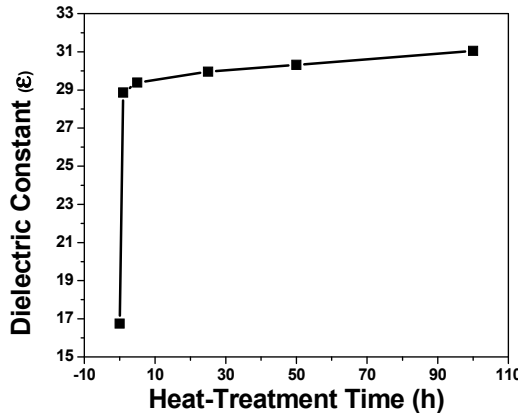


Fig. 17. Variation of dielectric constant of Er<sup>3+</sup> doped precursor KNS glass and KN nano glass-ceramics as a function of heat-treatment time.

### 6.7 UV-visible-NIR absorption spectra

Fig. 18 shows the representative UV-Vis-NIR absorption spectra of  $\text{Er}^{3+}$  doped precursor glass and heat-treated samples for 100 h duration. The absorption occurs due to the  $4f-4f$  electric dipole transitions from the ground  $^4I_{15/2}$  state to different excited state of  $\text{Er}^{3+}$  ions. The absorption spectra have very strong absorption edges below 350 nm and exhibit ten numbers of distinct absorption peaks which are similar to those appeared in silicate, tellurite and chloro sulphide glasses (Mandal et al., 2004, Bhaktha et al., 2006, Qian et al., 2008, Nayak et al., 2007, Lin et al., 2004, Schweizer et al., 1997). All the peaks were assigned in accordance with Carnall's convention as  $^4I_{15/2} \rightarrow ^2G_{9/2}$  (365 nm),  $^4G_{11/2}$  (377 nm),  $^2H_{9/2}$  (406 nm),  $^4F_{5/2} + ^4F_{3/2}$  (450 nm),  $^4F_{7/2}$  (488 nm),  $^2H_{11/2}$  (521 nm),  $^4S_{3/2}$  (544 nm),  $^4F_{9/2}$  (651 nm),  $^4I_{9/2}$  (799 nm) and  $^4I_{11/2}$  (978 nm) (Carnall et al., 1968). From this figure it is noticed that the base lines of the absorption spectra of heat-treated samples have been elevated significantly with diminishing intensities of the absorption peaks. The uplifting of the base line for glass-ceramic sample due to scattering imparted by the nanocrystallite phase is discussed as follows.

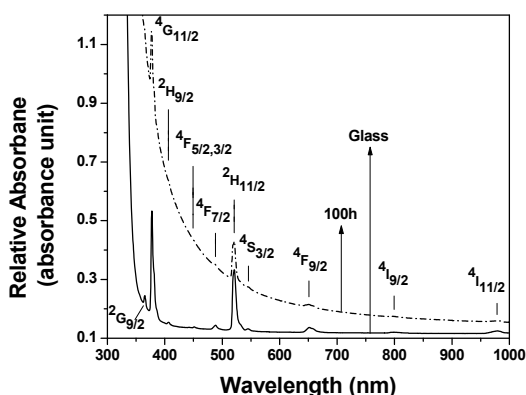


Fig. 18. Absorption spectra of the precursor KNS glass and glass heat-treated at 800°C for 100 h.

### 6.8 Photoluminescence spectra

Fig. 19 depicts the infrared emission spectra of precursor KNS glass and samples heat-treated for 2 and 100 h durations. The directly excited 980 nm emission spectra of the as prepared glass and the heat-treated samples exhibits emission from  $^4I_{13/2}$  excited level to the  $^4I_{15/2}$  ground level with Stark splitting at 1537 and 1566 nm. With increase in heat-treatment time the peak at 1537 nm for glass shifted to 1540 nm for 100 h heat-treated sample. The peak intensity ratio at 1566 nm to 1540 nm for precursor glass is  $\sim 0.93$  which decreases down to  $\sim 0.79$  for the heat-treated samples. It is generally seen that the glass-ceramics samples show more intense photoluminescence than the precursor glass. In this case it is found that the fluorescence intensity first decreases for the glass-ceramics heat-treated for shortest duration (2h) and then increases but with low intense than precursor glass. The reason behind this may be the fact that in the shorter durations of heat-treatment the samples are phase separated and stable  $\text{KNbO}_3$  phase grows with longer heat-treatment duration.

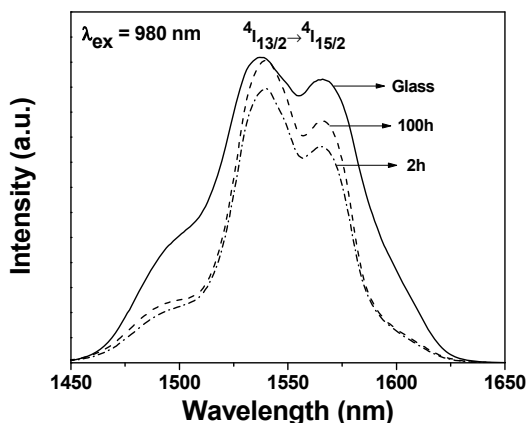


Fig. 19. (a) Near infrared emission spectra ( $\lambda_{\text{ex}} = 980 \text{ nm}$ ) of the precursor KNS glass and glasses heat-treated at  $800^\circ\text{C}$  for 2 and 100 h (a. u. = arbitrary unit).

### 6.9 Second harmonic generation (SHG)

The SHG output power (nJ) of KNS glass and KN glass-ceramics heat-treated at  $800^\circ\text{C}$  for 10 h is shown in Figs. 20(a) and (b). It is seen from the Fig. 20(a) that the precursor glass does not exhibit any SHG output. This phenomenon once again explained on the basis of inversion symmetry of the precursor glass. With heat-treatment of the precursor glass at  $800^\circ\text{C}$  for 10 h duration, the SHG output power increase to 39.74 nJ. This is attributed due to the formation of ferroelectric (non-centrosymmetric) KNbO<sub>3</sub> crystals in the glassy matrix.

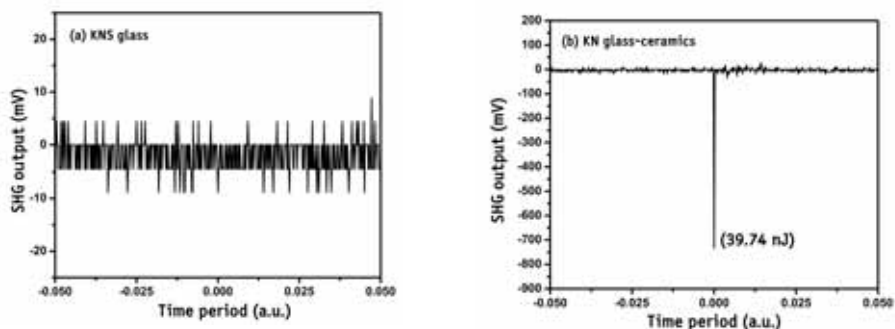


Fig. 20. Variation of SHG output power (nJ) with time period of precursor (a) KNS glass and (b)  $800^\circ\text{C}$  heat-treated for 10 h KN glass-ceramic sample.

## 7. Conclusions

The precursor glasses having molar composition  $25.53\text{Li}_2\text{O}-21.53\text{Ta}_2\text{O}_5-35.29\text{SiO}_2-17.65\text{Al}_2\text{O}_3$  doped with RE oxides (0.5 wt% of  $\text{Eu}_2\text{O}_3$  and  $\text{Nd}_2\text{O}_3$  in excess) and  $25\text{K}_2\text{O}-25\text{Nb}_2\text{O}_5-50\text{SiO}_2$  (KNS) doped with  $\text{Er}_2\text{O}_3$  (0.5 wt% in excess) were prepared by melt-quench technique. The precursor glasses and the resulting LT and KN nano glass-ceramics were characterized by

studying their thermal, structural, optical, dielectric properties. The results of XRD, FESEM, TEM and FT-IRRS confirmed the formation of nanocrystalline LT phases in the LTSA glass matrices and KN phase in the KNS glass matrix. The nanocrystallite size of LT and KN evaluated from TEM images found to vary in the range 14-36 nm and 5-12 nm respectively. The dielectric constants found to increase with heat-treatment time due to ferroelectric LT and KN formation. The photoluminescence studies indicate the incorporation of RE ions into LT and KN crystal lattice. The derived LT and KN nano glass-ceramics also exhibit considerable SHG output which is very important for exploitation in self frequency doubling laser devices.

## 8. References

- Abedin, K. S.; Tsuritani, T.; Sato, M. & Ito, H. (1997). Integrated intracavity quasi-phase-matched second harmonic generation based on periodically polled Nd:LiTaO<sub>3</sub>. *Appl. Phys. Lett.* 70, 1, 10-12, ISSN 0003-6951.
- Aronne, A. ; Sigaev, V. N. ; Pernice, P. ; Fanelli, E. & Usmanova, L. Z. (2004). Non-isothermal crystallization and nanostructuring in potassium niobium silicate glasses. *J. Non-Cryst. Solids*, 337, 2, 121-129, ISSN 0022-3093.
- Beall, G.H. & Duke, D. A. (1969). Transparent Glass-Ceramics. *J. Mater. Sci.* 4, 4, 340-352, ISSN 0022-2461.
- Beall, G. H. & Duke, D. A. (1983). *Glass-Ceramic Technology in Glass Science and Technology, Vol. 1: Glass-Forming Systems*, D.R. Uhlmann, N.J. Kreidl (Eds.), Academic Press, p. 403, ISBN 978-0127067018, New York,.
- Bhaktha, S. N. B.; Boulard, B. S.; Chausseudent, Chiappini, A.; Chiasera, A.; Duval, E.; Duverger, C.; Etienne, S.; Ferrari, M.; Jestin, Y.; Mattarelli, M.; Montagna, M.; Monteil, A.; Moser, E.; Portales, H. & Vishunubhatla, K. C. (2006). Erbium-activated modified silica glasses with high <sup>4</sup>I<sub>13/2</sub> luminescence quantum yield. *Opt. Mater.* 28, 11, 1325-1328, ISSN 0925-3467.
- Blech, I. A. (1986). *Properties of materials in electronics engineering handbook*, 2<sup>nd</sup> Edition, D.G. Fink, D. Christiansen Ed., McGraw-Hill, New York, p. 6-30.
- Burdick, V. L. & Day, D. E. (1967). Coordination of aluminium ions in tricalcium aluminate. *J. Am. Ceram. Soc.* 50, 2, 97-101, ISSN 1551-2916.
- Campbell, J. H. & Suratwala, T. I. (2000). Nd-doped phosphate glasses for high-energy/high-peak-power lasers. *J. Non-Cryst. Solids*, 263-264, 318-341, ISSN 0022-3093.
- Carnall, W. T.; Fields, P. R. & Rajnak, K. (1968). Electronic energy levels in the trivalent lanthanide aquo ions. I. Pr<sup>3+</sup>, Nd<sup>3+</sup>, Pm<sup>3+</sup>, Sm<sup>3+</sup>, Dy<sup>3+</sup>, Ho<sup>3+</sup>, Er<sup>3+</sup>, and Tm<sup>3+</sup>. *J. Chem. Phys.* 49, 10, 4424-4442.
- Chaliha, R. S.; Annapurna, K.; Tarafder, A.; Tiwari, V. S.; Gupta, P. K. & Karmakar, B. (2009). Luminescence and dielectric properties of nano-structured Eu<sup>3+</sup>:K<sub>2</sub>O-Nb<sub>2</sub>O<sub>5</sub>-SiO<sub>2</sub> glass-ceramics. *Solid State Sci.*, 11, 8, 1325-32, ISSN 1293-2558.
- Chaliha, R. S.; Annapurna, K.; Tarafder, A.; Tiwari, V. S.; Gupta, P. K. & Karmakar, B. (2010). Structure, dielectric and optical properties of transparent Nd<sup>3+</sup>: KNbO<sub>3</sub> nanocrystalline glass-ceramics. *Opt. Mater.* 32, 9, 1202-1209, ISSN 0925-3467.
- Chaliha, R. S.; Annapurna, K.; Tarafder, A.; Tiwari, V. S.; Gupta, P. K. & Karmakar, B. (2010). Optical and dielectric properties of isothermally crystallized nano KNbO<sub>3</sub> in Er<sup>3+</sup>-

- doped K<sub>2</sub>O-Nb<sub>2</sub>O<sub>5</sub>-SiO<sub>2</sub> glasses. *Spectrochim. Acta A Mol. Biomol. Spectrosc.* 75, 1, 243-250, ISSN 1386-1425.
- Chang, Y. M.; Yeom, T. H.; Yeung, Y. Y. & Rudowicz, C. (1993). Superposition model and crystal-field analysis of <sup>4</sup>A<sub>2</sub> and <sup>2</sup>E states of Cr<sup>3+</sup> ions at C<sub>3</sub> sites in LiNbO<sub>3</sub>. *J. Phys. C: Conds. Mater.* 5, 34, 6221-6230, ISSN 0953-8984.
- Chen, Y.; Huang, Y.; Huang, M.; Chen, R. & Luo, Z. (2005). Effect of Nd<sup>3+</sup> on the spectroscopic properties of bismuth borate glasses. *J. Am. Ceram. Soc.* 88, 1, 19-23, ISSN 0002-7820.
- Cheng, Z. X.; Kimura, H.; Ozawa, K.; Miyazaki, A. & Kanna, C. V. (2005). Ferroelectric lithium tantalate thin film derived from peroxide. *J. Alloys Compd.* 402, 1-2, 208-212, ISSN 0925-8388.
- Cullity, B. D. (1978). *Elements of X-ray diffraction*, 2<sup>nd</sup> Edition, Addison-Wesley Publishing Co., p. 101, ISBN-978-0201011746, London.
- Dai, S.; Wu, J.; Zhang, J.; Wang, G.; & Jiang, Z. (2005). The spectroscopic properties of Er<sup>3+</sup>-doped TeO<sub>2</sub>-Nb<sub>2</sub>O<sub>5</sub> glasses with high mechanical strength performance. *Spectrochim. Acta A Mol. Biomol. Spectrosc.* 62, 1-3, 431-437, ISSN 1386-1425.
- Dejneka, M. (1998). The luminescence and structure of novel transparent oxyfluoride glass-ceramics. *J. J. Non-Cryst. Solids*, 239, 1-3, 149-155, ISSN 0022-3093.
- de Andrade, J. S.; Pinheiro, A. G.; Vasconcelos, I. F.; deArujo, M. A. B.; Valente, M. A. & Sombra, A. S. B. (2000). Structural studies of KNbO<sub>3</sub> in niobate glass-ceramics. *J. Phys. Chem. Solids*, 61, 6, 899-906, ISSN 0022-3697.
- Fukumi, K. & Sakka, S. (1988). Coordination state of Nb<sup>5+</sup> ions in silicate and gallate glasses as studied by raman spectroscopy. *J. Mater. Sci.* 23, 8, 2819-2823, ISSN 0022-2461.
- Gasparotto, G.; Lima, S. A. M.; Davolos, M. R.; Varela, J. A.; Longo, E. & Zaghete, M. A. (2008). Luminescence properties of Eu<sup>3+</sup>- and Mg<sup>2+</sup>-doped LiTaO<sub>3</sub> obtained via the polymeric precursor method. *J. Lumin.* 128, 10, 1606-1610, ISSN 0022-3093.
- Golubkov, V. V.; Dymshits, O. S.; Zhilin, A. A.; Redin, A. V. & Shepilov, M. P. (2001). Crystallization of Glasses in the K<sub>2</sub>O-Nb<sub>2</sub>O<sub>5</sub>-SiO<sub>2</sub> System. *Glass Phys. Chem.* 27, 6, 504-511, ISSN 1087-6596.
- Gruber, J. B.; Allik, T. H.; Sardar, D. K.; Yow, R. M.; Scripsick, M. & Wechsler, B. (2006). Crystal growth and spectroscopic characterization of Yb<sup>3+</sup>:LiTaO<sub>3</sub>. *J. Lumin.* 117, 2, 233-238, ISSN 0022-2313.
- Hase, H.; Nasu, H.; Mito, A.; Hashimoto, T.; Matsuoka, J. & Kamiya, K. (1996). Second harmonic generation from surface crystallized Li<sub>2</sub>O-Ta<sub>2</sub>O<sub>5</sub>-SiO<sub>2</sub> glass. *Jpn. J. Appl. Phys.* 35, 10, 5355-5356, ISSN 0021-4922.
- Hirayama, C. & Berg, D. (1963). Dielectric properties of glasses in the system Nb<sub>2</sub>O<sub>5</sub>-Na<sub>2</sub>O-SiO<sub>2</sub>. *J. Am. Ceram. Soc.* 46, 2, 85-88, ISSN 1551-2916.
- Hui, Y. Y.; Shih, P-H.; Sun, K-J. & Lin, C-F. (2007). Enhancement of 1.5 μm emission in erbium-doped spin-on glass by furnace annealing. *Thin Solid Films.* 515, 17, 6754-6757, ISSN 0040-6090.
- Ito, S.; Kokubo, T. & Tashiro, M. (1978). Transparency of LiTaO<sub>3</sub>-SiO<sub>2</sub>-Al<sub>2</sub>O<sub>3</sub> glass-ceramics in relation to their microstructure. *J. Mater. Sci.* 13, 5, 930-938, ISSN 0022-2461.
- Jain, H. (2004). Transparent ferroelectric glass-ceramics. *Ferroelectrics*, 306, 111-127, ISSN 0015-0193.

- Kang, U.; Zhilin, A. A.; Logvinov, D. P.; Onushchenko, A. A.; Savost'yanov, V. A.; Chuvaeva, T. I. & Shashkin, A. V. (2001). Transparent Nd<sup>3+</sup>-activated glass-ceramics in the Li<sub>2</sub>O-Al<sub>2</sub>O<sub>3</sub>-SiO<sub>2</sub> system: physicochemical aspects of their preparation and optical characteristics. *Glass Phys. Chem.* 27, 4, 344-352, ISSN 1087-6596.
- Lin, H.; Liu, K.; Pun, E. Y. B.; Ma, T. C.; Peng, X.; An, Q. D.; Yu, J. Y. & Jiang, S. B. (2004). Infrared and visible fluorescence in Er<sup>3+</sup>-doped gallium tellurite glasses. *Chem. Phys. Lett.* 398, 1-3, 146-150, ISSN 0009-2614.
- Lynch, C. T. (1975). *CRC Handbook of Materials Science*, Vol. III, CRC Press, p. 170, Cleveland, Ohio.
- Mandal, D.; Banerjee, H. D.; Goswami, M. L. N. & Acharya, H. N. (2004). Synthesis of Er<sup>3+</sup> and Er<sup>3+</sup>:Yb<sup>3+</sup> doped sol-gel derived silica glass and studies on their optical properties. *Bull. Mater. Sci.* 27, 4, 367-372, ISSN 0250-4707.
- Mizuuchi, K. & Yamamoto, K. (1995). Harmonic blue light generation in bulk periodically poled LiTaO<sub>3</sub>. *Appl. Phys. Lett.* 66, 22, 2943-2945, ISSN 0003-6951.
- Moses, A. J. (1978). *The practicing scientist's handbook*. Van Nostrand Reinhold Company, p. 558, ISBN 0442 25584 5 New York.
- Mukherjee, P. & Varma, K. B. R. (2004). Crystallization and physical properties of LiTaO<sub>3</sub> in a reactive glass matrix (LiBO<sub>2</sub>-Ta<sub>2</sub>O<sub>5</sub>). *Ferroelectrics*, 306, 1, 129-143, ISSN 0015-0193.
- Naranjo, B.; Gimzewski, J. K. & Putterman, S. (2005). Observation of nuclear fusion driven by a pyroelectric crystal. *Nature*, 434, 1115-1117, ISSN 0028-0836.
- Nayak, A.; Kundu, P. & Debnath, R. (2007). Strong green emission from Er<sup>3+</sup> in a fluorine containing (Pb, La)-tellurite glass without using up-conversion route. *J. Non. Cryst. Solids*, 353, 13-15, 1414-1417, ISSN 0022-3093.
- Ono, H.; Hosokawa, Y.; Shinoda, K.; Koyanagi, K. & Yamaguchi, H. (2001). Ta-O phonon peaks in tantalum oxide films on Si. *Thin Solid Films*, 381, 1, 57-61, ISSN 0040-6090.
- Palik, E. D. (1997) *Handbook of optical constants of solids III*, Academic Press, p. 834, ISBN 0125444230, San Diego.
- Pátek, K. (1970). *Glass Lasers*, Butterworth & Co (Publishers) Ltd., p.95, ISBN 978-0592027784, London.
- Pernice, P.; Aronne, A.; Sigaev, V. N.; Sarkisov, P. D.; Molev, V. I. & Stefanovich, S. Y. (1999). Crystallization behavior of potassium niobium silicate glasses. *J. Am. Ceram. Soc.* 82, 12, 3447-3452, ISSN 0002-7820.
- Pernice, P.; Aronne, A.; Sigaev, V. N. & Kupriyanova, M. (2000). Crystallization of the K<sub>2</sub>O·Nb<sub>2</sub>O<sub>5</sub>·2SiO<sub>2</sub> glass: evidences for existence of bulk nanocrystalline structure. *J. Non-Cryst. Solids*, 275, 3, 216-224, ISSN 0022-3093.
- Qian, Q.; Wang, Y.; Zhang, Q. Y.; G. F.; Yang, Yang, Z. M. & Jiang, Z. H. (2008). Spectroscopic properties of Er<sup>3+</sup>-doped Na<sub>2</sub>O-Sb<sub>2</sub>O<sub>3</sub>-B<sub>2</sub>O<sub>3</sub>-SiO<sub>2</sub> glasses. *J. Non. Cryst. Solids*, 354, 18, 1981-1985, ISSN 0022-3093.
- Riello, P.; Bucella, S.; Zamengo, L.; Anselmi-Tamburini, U.; Francini, R.; Pietrantoni, S.; & Munir, Z. A. (2006). Erbium-doped LAS glass ceramics prepared by spark plasma sintering (SPS). *J. Eur. Ceram. Soc.* 26, 15, 3301-3306, ISSN 0955-2219.
- Ringgaard, E. & Wurlitzer, T. (2005). Lead-free piezoceramics based on alkali niobates. *J. Eur. Ceram. Soc.* 25, 12, 2701-2706, ISSN 0955-2219.
- Risk, W. P.; Gosnell, T. R. & Nurmikko, A. V. (2003). *Compact blue-green lasers*, Cambridge University Press, ISBN 9780521623186, Cambridge.

- Romanowski, W. R.; Sokólska, I.; Dzik, G. D. & Gołab, S. (2000). Investigation of LiXO<sub>3</sub> (X=Nb, Ta) crystals doped with luminescent ions: Recent results. *J. Alloys Compd.* 300-301, 152-157, ISSN 0925-8388.
- Samuneva, B.; Kralchev, St. & Dimitrov, V. (1991). Structure and optical properties of niobium silicate glasses. *J. Non-Crys. Solids*, 129, 1-3, 54-63, ISSN 0022-3093.
- Schweizer, T.; Brady, D. J. & Hewak, D. W. (1997). Fabrication and spectroscopy of erbium doped gallium lanthanum sulphide glass fibres for mid-infrared laser applications. *Opt. Exp.* 1, 4, 102-107, ISSN 1094-4087.
- Silva, E. N.; Ayala, A. P.; Guedes, I.; C. Paschoal, W. A.; Moreira, R. L.; C. -K. Loong, & Boatner, L. A. (2006). Vibrational spectra of monazite-type rare-earth orthophosphates. *Opt. Mater.* 29, 2-3, 224-230, ISSN 0925-3467.
- Simões, A. Z.; Ries, A.; Riccardi, C. S.; Gonzalez, A. H.; Zaghete, M. A.; Stojanovic, Cilense, B. D. M. & Varela, J. A. (2004). Potassium niobate thin films prepared through polymeric precursor method. *Mat. Lett.* 58, 20, 2537-2540, ISSN 0167-577X.
- Sokólska, I. (2002). Infrared to visible conversion of radiation in some Ho<sup>3+</sup>-doped oxide and fluoride crystals. *J. Alloys Compd.* 341, 1-2, 288-293, ISSN 0925-8388.
- Sokólska, I.; Kück, S.; Dzik, G. D. & Baba, M. (2001). The up-conversion processes in Ho<sup>3+</sup> doped LiTaO<sub>3</sub>. *J. Alloys Compd.* 323-324, 273-278, ISSN 0925-8388.
- Tanaka, H.; Yamamoto, M.; Takahashi, Y.; Benino, Y.; Fujiwara, T. & Komatsu, T. (2003). Crystalline phases and second harmonic intensities in potassium niobium silicate crystallized glasses. *Opt. Mater.* 22, 1, 71-79, ISSN 0925-3467.
- Tarafder, A.; Annapurna, K.; Chaliha, R. S.; Tiwari, V. S.; Gupta, P. K. & Karmakar, B. (2009). Processing and properties of Eu<sup>3+</sup>:LiTaO<sub>3</sub> transparent glass-ceramic nanocomposites. *J. Am. Ceram. Soc.* 92, 9, 1934-1939, ISSN 0002-7820.
- Tarafder, A.; Annapurna, K.; Chaliha, R. S.; Tiwari, V. S.; Gupta, P. K. & Karmakar, B. (2010). Structure, dielectric and optical properties of Nd<sup>3+</sup> doped LiTaO<sub>3</sub> transparent ferroelectric glass-ceramic nanocomposites. *J. Alloys Compd.* 489, 1, 281-288, ISSN 0925-8388.
- Tarafder, A.; Annapurna, K.; Chaliha, R. S.; Tiwari, V. S.; Gupta, P. K. & Karmakar, B. (DOI:10.1111/j.1744-7402.2010.02494.x). Effects of nano LiTaO<sub>3</sub> crystallization on dielectric and optical properties in Er<sup>3+</sup>-doped Li<sub>2</sub>O-Ta<sub>2</sub>O<sub>5</sub>-SiO<sub>2</sub>-Al<sub>2</sub>O<sub>3</sub> glasses. *Int. J. Appl. Ceram. Technol.*
- Tarafder, A.; Annapurna, K.; Chaliha, R. S.; Satapathy, S.; V. Tiwari, S.; Gupta, P. K. & Karmakar, B. (2011). Second harmonic generation in ferroelectric LiTaO<sub>3</sub> and KNbO<sub>3</sub> containing bulk nano glass-ceramics. *J. Nonlinear Opt. Phys. Mater.* 20, 1, 49-61, ISSN 0218-8635.
- Vernacotola, D. E. (1994). Alkali Niobium and Tantalum Silicate Glasses and Ferroelectric Glass-Ceramics. *Key Engg. Mater.* 94-95, 379-408.
- Vernacotola, D. E. & Shelby, J. E. (1994). Potassium niobium silicate glasses. *Phys. Chem. Glasses*, 35, 4, 153-159, ISSN 0031-9090.
- Volf, M. B. (1984). *Chemical approach to glass*, Elsevier, p.125, ISBN 0444996354, Amsterdam.
- Wu, S. Y. & Zheng, W. C. (2002). EPR parameters and defect structures for two trigonal Er<sup>3+</sup> centers in LiNbO<sub>3</sub> and MgO or ZnO codoped LiNbO<sub>3</sub> crystals. *Phys. Rev. B*, 65, 22, 224107-1-6, ISSN 0163-1829.
- Winburn, D. C. (1985). *Practical Laser Safety*, Dekker, ISBN 0824773489, New York.

- Wu, S. Y. & Dong, H. N. (2005). Studies of the EPR g factors and the local structure for the trigonal  $\text{Nd}^{3+}$  center in  $\text{LiNbO}_3:\text{Nd}^{3+}$  crystal. *J. Alloy. Comp.*, 386, 1-2, 52-56, ISSN 0925-8388.
- Xue, D. & Zhang, S. (1998). Linear and nonlinear optical properties of  $\text{KNbO}_3$ . *Chem. Phys. Lett.* 291, 3-4, 401-406 ISSN 0009-2614.
- Yamane, M. & Asahara, Y. (2000). *Glasses for photonics*, Cambridge University Press, p.173, ISBN 0 521 58053 6, Cambridge, UK.
- Youssef, S.; Asmar, R. Al., Podlecki, J.; Sorli, B. & Foucaran, A. (2008). Structural and optical characterization of oriented  $\text{LiTaO}_3$  thin films deposited by sol-gel technique. *Eur. Phys. J. Appl. Phys.* 43, 1, 65-71, ISSN 1286-0042.
- Zgonik, M.; Schlessner, R.; Biaggio, I.; Voit, E.; Tscherry, J. & Giinter, P. (1993). Materials constants of  $\text{KNbO}_3$  relevant for electro- and acousto-optics. *J. Appl. Phys.* 74, 2, 1287-1297, ISSN 0021-8979.
- Zhang, J. Y.; Boyd, I. W.; Dusastre, V. & Williams, D. E. (1999). Ultraviolet annealing of tantalum oxide films grown by photo-induced chemical vapor deposition. *J. Phys. D: Appl. Phys.* 32, 19, L91-95, ISSN 0022-3727.
- Zheng, F.; Liu, H.; Liu, D.; Yao, S.; Yan, T. & Wang, J. (2009). Hydrothermal and wet-chemical synthesis of pure  $\text{LiTaO}_3$  powders by using commercial tantalum hydroxide as starting material. *J. Alloys Compd.* 477, 1-2, 688-691, ISSN 0925-8388.
- Zhu, S.; Zhu, Y.; Yang, Z.; Wang, H.; Zhang, Z.; Hong, J.; Ge, C. & Ming, N. (1995). Second-harmonic generation of blue light in bulk periodically poled  $\text{LiTaO}_3$ . *Appl. Phys. Lett.* 67, 3, 320-322, ISSN 0003-6951.